SIAM J. APPL. MATH.
Vol. 76, No. 3, pp. 930–949

A MACROSCOPIC MODEL FOR THE DIFFUSION MRI SIGNAL ACCOUNTING FOR TIME-DEPENDENT DIFFUSIVITY*

HOUSSEM HADDAR†, JING-REBECCA LI†, AND SIMONA SCHIAVI†

Abstract. Diffusion magnetic resonance imaging (dMRI) encodes water displacement due to diffusion and is a powerful tool for obtaining information on the tissue microstructure. An important quantity measured in dMRI in each voxel is the apparent diffusion coefficient (*ADC*), and it is well established from imaging experiments that, in the brain, in vivo, the *ADC* is dependent on the measured diffusion time. To aid in the understanding and interpretation of the *ADC*, using homogenization techniques, we derived a new asymptotic model for the dMRI signal from the Bloch–Torrey equation governing the water proton magnetization under the influence of diffusion-encoding magnetic gradient pulses. Our new model was obtained using a particular choice of scaling for the time, the biological cell membrane permeability, the diffusion-encoding magnetic field gradient strength, and a periodicity length of the cellular geometry. The *ADC* of the resulting model is dependent on the diffusion time. We numerically validated this model for a wide range of diffusion times for two-dimensional geometrical configurations.

Key words. diffusion MRI, time-dependent diffusivity, *ADC*, homogenization

AMS subject classifications. 35B27, 35Q99, 65M32, 65Z05

DOI. 10.1137/15M1019398

1. Introduction.

The image contrast in water proton diffusion magnetic resonance imaging (dMRI) comes from the differing average water displacement due to diffusion in the imaged tissue at different spatial positions [19]. A major application has been in detecting acute cerebral ischemia minutes after stroke [27, 44]. DMRI has been used to detect and differentiate a wide range of physiological and pathological conditions in the brain, including tumors [25, 39, 43] and myelination abnormalities (for a review, see [20]). It also has been used to study brain connectivity (for a review, see [18]) and in functional imaging [21] as well as in cardiac applications [7, 8, 36].

An ideal dMRI experiment consists in applying two very short pulses, each of duration δ, of the gradient magnetic field $B = \mathbf{g} \cdot \mathbf{x}$, with a 180 degree spin reversal between the two pulses, in order to encode the average water displacement in the imaged sample due to diffusion in the direction of $\mathbf{g}$, during the measured diffusion time of Δ, where Δ denotes the delay between the start of the two pulses [38]. The assumption that the pulse duration is short, $\delta \ll \Delta$, is called the narrow pulse assumption, and under this assumption the concept of diffusion time is unambiguous.

Under the narrow pulse assumption, after the first pulse, the complex phase due to spins that were at position $\mathbf{x}_0$ before the pulse is $e^{i\delta\gamma\mathbf{g}\cdot\mathbf{x}_0}$, where $\gamma = 42.576$ MHz/Tesla is the gyromagnetic ratio of the water proton. Because the gradient magnetic field is turned off after the first pulse, the phase of the spins does not change until the application of the radio-frequency (RF) pulse to apply the 180 degree spin reversal. After the 180 degree RF pulse, the complex phase becomes $e^{-i\delta\gamma\mathbf{g}\cdot\mathbf{x}_0}$. The phase of the spins stays the same until the application of the second pulse, after which the complex phase due to spins ending up at position $\mathbf{x}_f$ becomes $e^{i\delta\gamma\mathbf{g}\cdot(\mathbf{x}_f-\mathbf{x}_0)}$. The dMRI signal S (total water proton magnetization in a physical volume V, called a

*Received by the editors May 5, 2015; accepted for publication (in revised form) March 1, 2016; published electronically May 17, 2016.
http://www.siam.org/journals/siap/76-3/M101939.html
†INRIA-Saclay, Equipe DeFI, CMAP, Ecole Polytechnique, 91128 Palaiseau Cedex, France (houssem.haddar@inria.fr, jingrebecca.li@inria.fr, simona.schiavi@inria.fr).

voxel) due to the spins originally at $\mathbf{x}_0$ is

$$S = \int_V P(\mathbf{x}, \mathbf{x}_0, \Delta)\rho(\mathbf{x}_0)e^{i\delta\gamma\mathbf{g}\cdot(\mathbf{x}-\mathbf{x}_0)}d\mathbf{x},$$

where $P(\mathbf{x}, \mathbf{x}_0, \Delta)$ is the proportion of the original spins starting at $\mathbf{x}_0$ that end up at $\mathbf{x}$ a time Δ later and $\rho(\mathbf{x}_0)$ is the density of spins at $\mathbf{x}_0$. If water is freely diffusing with the isotropic diffusion coefficient σ, then

$$P(\mathbf{x}, \mathbf{x}_0, \Delta) = \frac{e^{-\frac{\|\mathbf{x}-\mathbf{x}_0\|^2}{4\pi\sigma\Delta}}}{(4\pi\sigma\Delta)^{3/2}}$$

is the diffusion (heat) Green's function in free space. If we assume the diffusion displacement is small compared to the side lengths of the voxel (which is true for dMRI), then using the well-known result about the Fourier transform of P we obtain

$$S = \rho(\mathbf{x}_0)e^{-\sigma\|\gamma\delta\mathbf{g}\|^2\Delta}, \tag{1.1}$$

where the Fourier variable is $\gamma\delta\mathbf{g}$. We will denote

$$q := \|\gamma\mathbf{g}\|$$

and the gradient direction by

$$\mathbf{u_g} := \mathbf{g}/\|\mathbf{g}\|.$$

In the general case, without the narrow pulse assumption, it is easy to show that the signal is

$$S = \rho(\mathbf{x}_0)e^{-\sigma q^2\delta^2(\Delta-\delta/3)}. \tag{1.2}$$

Though the notion of the measured diffusion time is ambiguous without the narrow pulse assumption, the MR community has variously used the term diffusion time to mean Δ, $\Delta - \delta/3$, or $\Delta + \delta$. In this paper, we will use the phrase "diffusion time–dependent" to mean dependent on Δ and δ.

An important quantity in dMRI is the apparent diffusion coefficient (ADC), and it is usually obtained by measuring S for a given Δ, δ, $\mathbf{u_g}$ at several values of q and fitting the following formula:

$$\log S = \log S_0 - (ADC)q^2\delta^2(\Delta - \delta/3), \tag{1.3}$$

where S_0 is the dMRI signal when $q = 0$. Obviously, $ADC = \sigma$ in the case of free diffusion.

In the context of dMRI, brain tissue diffusion is not free, and this is evidenced by the fact that the fitted ADC depends on the applied gradient strength $\|\mathbf{g}\|$, its direction $\mathbf{u_g}$, and diffusion time (Δ and δ). In fact, it is hoped that a signal model more accurate and complicated than (1.2) would provide additional information on the tissue microstructure. As a consequence, there have been many proposed extensions to (1.2), formulated heuristically, by dMRI researchers. For example, the dMRI signal as a sum of multiple exponentials was proposed in [10, 24, 28, 30], a term that is $O(q^4\delta^4(\Delta - \delta/3)^2)$ was added to (1.3) in [6, 14], and P was replaced by fractional

order diffusion in [5, 22, 23]. In [46], the signal model is an integral of a continuum of Gaussian diffusion groups, each with a different effective diffusion coefficient. In [33] the signal model is an expansion in a perturbation of the mean diffusivity. The models of [3, 15, 37] separate the cylindrical-shaped axons and dendrites from the space outside them to make two diffusion compartments and assume there is no water exchange between them. The Karger model [16] supposes multiple Gaussian diffusion compartments, where the water exchange between the compartments is described by simple constant rate terms that can be added to the diffusion terms, and these assumptions enable the formulation of a system of coupled ordinary differential equations (ODEs) that describes the time evolution of the total magnetization in the different compartments.

The previously mentioned models can be characterized as phenomenological models that incorporate certain physical assumptions and insights about the spatial and time scales of water diffusion in a complex geometrical environment. On the other hand, one can also proceed mathematically starting from a detailed and accurate description using partial differential equations (PDEs). The Bloch–Torrey PDE [42] can be used to describe the water proton magnetization at all spatial positions in a voxel once the positions and shapes of the biological cells and the permeability of the cell membranes are prescribed. Obviously, this very accurate microscopic description cannot be used as a practical model of the dMRI signal because its inputs—the complete geometrical description of the biological cells in a voxel and its immediate neighbors—are too complicated compared to the physically obtainable data. This is the motivation for formulating asymptotic models from the Bloch–Torrey PDE.

Two simple asymptotic models are the following. In the short time limit where only a small fraction of random walkers have encountered the membrane, the signal model given in [31], which is a general case of the formula in [26], is

$$\log S_{short} := \log S_0 + D_{short}(\Delta) q^2 \delta^2(\Delta), \tag{1.4}$$

where the diffusion time–dependent effective diffusion coefficient $D_{short}(\Delta)$ in the presence of multiple geometrical subdomains Y_j, each with boundary Γ_{jk} and intrinsic diffusion coefficient σ_j, is

$$D_{short}(\Delta) := \sum_j v_j D^j_{short}(\Delta), \tag{1.5}$$

where v_j is the volume fraction of subdomain Y_j and

$$D^j_{short}(\Delta) := \sigma_j \left[1 - \frac{|\Gamma_j|}{d|Y_j|} \left(\frac{4\sqrt{\sigma_j \Delta}}{3\sqrt{\pi}} - \kappa \Delta \right) \right], \tag{1.6}$$

d being the space dimension, and κ is the membrane permeability.

In the long time limit when the diffusion becomes effectively Gaussian, then the signal model is exponential:

$$\log S_{long} := \log S_0 - ({\mathbf{u_g}}^T \overline{D}_{long} \mathbf{u_g}) q^2 \delta^2 (\Delta - \delta/3), \tag{1.7}$$

where $\overline{D}_{long} \in \mathbb{R}^d \times \mathbb{R}^d$ is the long time effective diffusion tensor. It was shown in [9] that in the case of periodic media, where $Y = \prod_{i=1\cdots d}[0, L_i]$ is a periodicity box of the medium, then

$$\left(\overline{D}_{long}\right)_{il} := \frac{1}{|Y|} \sum_j \int_{Y_j} \sigma_j(\mathbf{x}) \nabla u^j_i(\mathbf{x}) \cdot \mathbf{e}_l \, d\mathbf{x}, \tag{1.8}$$

where the functions $u_i^j(\mathbf{x})$, $i = 1, \ldots, d$, are defined piecewise on Y_j and satisfy the time-independent PDE:

$$
\begin{aligned}
\operatorname{div}\big(\sigma_j(\mathbf{x})\nabla u_i^j(\mathbf{x})\big) &= 0 && \text{in } Y_j,\\
\sigma_j(\mathbf{x})\nabla u_i^j(\mathbf{x})\cdot\nu - \sigma_k(\mathbf{x})\nabla u_i^k(\mathbf{x})\cdot\nu &= 0 && \text{on } \Gamma_{jk},\\
\sigma_j(\mathbf{x})\nabla u_i^j(\mathbf{x})\cdot\nu &= \kappa(u_i^j(\mathbf{x}) - u_i^k(\mathbf{x})) && \text{on } \Gamma_{jk},\\
u_i^j(\mathbf{x} + L_i\mathbf{e}_i) &= u_i^j(\mathbf{x}) + L_i && \text{on } \partial Y,\\
u_i^j(\mathbf{x} + L_l\mathbf{e}_l) &= u_i^j(\mathbf{x}), \quad l \neq i, && \text{on } \partial Y.
\end{aligned}
\tag{1.9}
$$

If Y only contains simple geometries such as cubes and spheres, analytic formulae for $\overline{D}_{long}$ have been formulated [13, 17, 40, 41].

In a previous work [11] we derived an asymptotic model from the Bloch–Torrey equation using periodic homogenization techniques by choosing a particular scaling of time, the membrane permeability, the diffusion-encoding gradient amplitude, and a periodicity length of the medium. The resulting model is valid for long diffusion times when the signal may nevertheless exhibit a non-Gaussian behavior due to water exchange between the subdomains. The assumption of low membrane permeability means the exchange is governed by linear kinetics and gives the signal model a particularly simple form as the solution of a system of coupled ODEs. Indeed, it was found that this model generalizes the Karger model, which was a dMRI signal model formulated heuristically by physicists for long diffusion times, but which is subject to the restriction that the duration of the pulses of a diffusion-encoding sequence is much shorter than the delay between the pulses. In contrast to the Karger model, our model in [11] is not restricted to the case where the pulse duration is small. For this reason we named our model the finite-pulse Karger (FPK) model.

A deficiency of the Karger and the FPK signal models is that they do not reproduce the experimentally observed (see [35] and the references contained therein) dependence of the *ADC* on Δ (and δ in the nonnarrow pulse case).

For this reason, in this paper, we chose a scaling different from that used to derive the FPK model, and we derived a new asymptotic dMRI signal model whose *ADC* depends on Δ and δ, again using periodic homogenization. We numerically validate, in some two-dimensional geometries, that the *ADC* of the new asymptotic model is a good approximation of the *ADC* of the Bloch–Torrey PDE description over a wide range of Δ and δ. We note that even though our new asymptotic model is derived using periodic homogenization, the use of the model is not limited to periodic domains. We cite the nonperiodic homogenization approach in porous media [1, 2], where the difference between the periodic and the nonperiodic cases is in the definition and interpretation of the macroscopic model coefficients.

Our new asymptotic model requires the solution of several homogeneous diffusion equations with source terms defined on the biological cell membranes. Unlike in [11], we could not put this model in the form of a system of coupled ODEs. However, we believe that this model can be further simplified since homogeneous diffusion equations with boundary sources terms have been extensively studied in the literature, and this will be the focus of future work. We believe that a mathematical homogenization approach is a useful complement to the phenomenological approach used by physicists, as seen by the FPK model of [11], formulated by homogenization, that elucidates and generalizes the phenomenological Karger model. It is very possible that the new asymptotic model that we derive in this paper can elucidate results about the time-dependent diffusivity in heterogeneous media obtained by physicists (see, for example,

[31, 32]). The novel result of this paper is a time-dependent *ADC* model that can lend itself to systematic mathematical analysis. It is hoped that future work in the analysis of this new *ADC* model will lead to a characterization of the time-dependent *ADC* in terms of tissue-related quantities such as the average surface to volume ratio and the dominant Laplace eigenfunctions of the biological cells that are contained in an imaging voxel. The ultimate goal is of course the estimation of these tissue-related quantities from the measured dMRI signal.

This paper is organized as follows. Section 2 introduces the Bloch–Torrey PDE that describes the complex transverse water proton magnetization due to diffusion-encoding magnetic field gradient pulses and poses the problem on the microscopic scale in a heterogeneous domain. For simplicity, we make the hypothesis that the domain to be modeled is periodic, which allows us to apply periodic homogenization theory. In section 3 we make the formal homogenization of our model problem in the periodic context, using a particular choice of scaling for the time, the biological cell membrane permeability, the diffusion-encoding magnetic field gradient strength, and the periodicity length of the cellular geometry. We give the description of our asymptotic dMRI signal model and its *ADC*. In section 4 we numerically validate the asymptotic model for some two-dimensional geometrical configurations. We show the convergence for both the signal and the *ADC*. We then show that the *ADC* of our new model is a good approximation of the *ADC* of the reference model (the microscopic description using the Bloch–Torrey PDE) over a wide range of times. Section 5 contains our conclusions.

2. Problem setting. For a volume $\Omega \subset \mathbb{R}^d$ of biological tissue, we denote by $\Gamma_I \subset \mathbb{R}^{d-1}$ the union of the boundaries of biological cells, in other words, the cell membranes, in Ω. In this paper, we assume the cell membranes are represented as $(d-1)$-dimensional objects. The cell membranes Γ_I thus delimit two subdomains: the extracellular domain Ω_e (e for extracellular) and the intracellular domain Ω_c (c for cellular). The domain Ω_{ext} then represents the union of the extracellular and intracellular open domains:

$$\Omega_{ext} \;\equiv\; \Omega \setminus \Gamma_I \;\equiv\; \Omega_e \cup \Omega_c\,.$$

2.1. Bloch–Torrey equation. The complex transverse water proton magnetization M can be described by the following Bloch–Torrey PDE [42] with the jump on Γ_I:

(2.1)
$$\begin{cases} \dfrac{\partial}{\partial t}M(\mathbf{x},t) + \iota q \mathbf{u_g}\cdot\mathbf{x} f(t) M(\mathbf{x},t) - \operatorname{div}(\sigma(\mathbf{x})\nabla M(\mathbf{x},t)) = 0 & \text{in } \Omega_{ext}\times]0,T[\,, \\ \sigma\nabla M\cdot\nu|_{\Gamma_I} = \kappa[\![M]\!]_{\Gamma_I} & \text{on } \Gamma_I, \\ [\![\sigma\nabla M\cdot\nu]\!]_{\Gamma_I} = 0 & \text{on } \Gamma_I, \\ M(\cdot,0) = M_{\text{ini}} & \text{in } \Omega_{ext}\times]0,T[\\ \text{and appropriate boundary conditions on } \partial\Omega, \end{cases}$$

where ν is the exterior normal to Ω_c, $[\cdot]_{\Gamma_I}$ is the jump (extracellular minus intracellular) on Γ_I, κ is the membrane permeability coefficient, ι is the imaginary unit, and M_{init} is the initial magnetization. The physical meaning of the parameter q is $q = \|\gamma\mathbf{g}\|$, where γ is the gyromagnetic ratio of the water proton, $\mathbf{g}$ gives the amplitude and direction of the diffusion-encoding gradient, and $\mathbf{u_g} = \mathbf{g}/\|\mathbf{g}\| \in \mathbb{R}^d$ is the unit vector in the direction of $\mathbf{g}$.

For simplicity of notation, the microscopic scale diffusion is assumed to be isotropic, and hence it is described by an intrinsic diffusion coefficient $\sigma(\mathbf{x}) \in \mathbb{R}$ rather than a tensor. The case of the tensor can be treated in a similar way but with more cumbersome notation. The function $f(t)$ gives the time profile of the diffusion-encoding magnetic field gradient pulses. For the classic pulsed gradient spin echo (PGSE) sequence [38], simplified to include only the parameters relevant to diffusion (the imaging gradients are ignored),

$$f(t) = \begin{cases} 1, & t_s < t \le t_s + \delta, \\ -1, & t_s + \Delta < t \le t_s + \Delta + \delta, \\ 0 & \text{elsewhere}, \end{cases}$$

where t_s is the start of the first pulse and we made $f(t)$ negative in the second pulse to include the effect of the 180 degree spin reversal between the pulses. The time at which the signal is measured is called the echo time $T_E \ge \delta + \Delta$. For simplicity, since t_s does not play a role in the results of this paper, we set $t_s = 0$. For the same reason, we set $T_E = \delta + \Delta$ in this paper. The dMRI signal is then the total magnetization at $t = \delta + \Delta$:

$$S = \int_V M(\mathbf{x}, \delta + \Delta) d\mathbf{x}, \tag{2.2}$$

where M is the solution of (2.1), and V is the voxel. We observe that, because the diffusion displacement in dMRI ($O(10\mu m)$) is usually very small compared to the size of the voxel ($O(1mm)$), the boundary conditions on $\partial\Omega$ in (2.1) can be any appropriate artificial boundary conditions because the support of the solution will be away from $\partial\Omega$ during the simulation time. The logarithm of the signal is usually plotted against a quantity called the b-value,

$$b := q^2 \int_0^{\Delta+\delta} \left(\int_0^t f(s)\, ds \right)^2 dt = q^2 \delta^2 \left(\Delta - \frac{\delta}{3} \right), \tag{2.3}$$

because in a homogeneous medium,

$$\log S = \log S_0 - \sigma\, b. \tag{2.4}$$

The b-value is a very important quantity in dMRI because the b-values are usually kept constant across different experiments. For different choices of Δ and δ, the values of q are adjusted according to (2.3) so that the same set of b-values is used to compute the dMRI signal. The range of b-values is usually chosen so that the signal attenuation, S/S_0, varies in a physically detectable range. This range will depend on the application and tissue type (brain, heart, etc.).

To obtain the ADC from a dMRI experiment, one fixes the choice of Δ and δ, computes the necessary q's to obtain several b-values that give an attenuation S/S_0 that is not too small (closer to 1 than to 0), and computes the slope of $\log S$ versus the b-values. To make the concept of the ADC mathematically rigorous, we choose the following definition:

$$ADC := -\frac{1}{\delta^2(\Delta - \delta/3)} \frac{\partial(\log S)}{\partial(q^2)}\bigg|_{q^2=0}, \tag{2.5}$$

where the analytical derivative of $\log S$ is taken at $q^2 = 0$ (while Δ and δ are fixed). We can write the derivative with respect to q^2 because, due to the symmetry of

diffusion, only even powers of q appear in S. With this definition, we note that ADC may depend on $\mathbf{u_g}$ and time (Δ and δ). In the narrow pulse limit, in a heterogeneous medium, the physical meaning of ADC is that it is the mean squared distance traveled by water molecules (averaged over all starting positions) divided by 2Δ.

2.2. Periodicity length. We will use the techniques of periodic homogenization. This means we will assume that the volume to be modeled, Ω, can be described as a periodic domain: there exists a period εL_0, which represents the average size of a representative volume of Ω and which is small compared to the size of Ω. For simplicity, we will assume the periodicity box is a cube. We define the normalized periodicity box to be $Y = [0, L_0]^d$ and let $Y = Y_e \cup Y_c$, where Y_e is the extracellular domain and Y_c is the intracellular domain. Y_c is an open set that may be made of several disconnected parts. We denote the boundary of Y_c by $\partial Y_c \equiv \Gamma_m$. We thus have

$$\Omega_e^\varepsilon = \bigcup_{\mathbf{z}\in\mathbb{Z}^d} \varepsilon(Y_e + \mathbf{z}L_0), \quad \Omega_c^\varepsilon = \bigcup_{\mathbf{z}\in\mathbb{Z}^d} \varepsilon(Y_c + \mathbf{z}L_0), \quad \Omega_{ext}^\varepsilon = \Omega_e^\varepsilon \cup \Omega_c^\varepsilon,$$
$$\text{and} \quad \Gamma_m^\varepsilon = \partial\Omega_e^\varepsilon \setminus \overline{\partial\Omega} = \bigcup_{\mathbf{z}\in\mathbb{Z}^d} \varepsilon(\Gamma_m + \mathbf{z}L_0).$$

Of course, the diffusion coefficient will be assumed to be periodic as well; i.e., there exists $\hat{\sigma} \in L^\infty(Y)$ such that $\sigma(\mathbf{x}) = \hat{\sigma}(\frac{\mathbf{x}}{\epsilon})$, with

$$\hat{\sigma} = \begin{cases} \sigma_e & \text{in } Y_e, \\ \sigma_c & \text{in } Y_c. \end{cases}$$

The most common and practical choice for σ_e and σ_c is to consider them both as constant so that $\hat{\sigma}$ is piecewise constant. With this more precise description of the domain, our reference model can be rewritten as

(2.6)
$$\begin{cases} \frac{\partial}{\partial t} M_\varepsilon(\mathbf{x},t) + \iota q\, \mathbf{u_g}\cdot\mathbf{x} f(t) M_\varepsilon(\mathbf{x},t) - \operatorname{div}(\hat{\sigma}_\varepsilon \nabla M_\varepsilon(\mathbf{x},t)) = 0 & \text{in } \Omega_{ext}^\varepsilon \times]0,T[, \\ \hat{\sigma}_\varepsilon \nabla M_\varepsilon \cdot \nu|_{\Gamma_m^\varepsilon} = \kappa^\varepsilon [\![M_\varepsilon]\!]_{\Gamma_m^\varepsilon}, & \\ [\![\hat{\sigma}_\varepsilon \nabla M_\varepsilon \cdot \nu]\!]_{\Gamma_m^\varepsilon} = 0, & \\ M_\varepsilon(\cdot,0) = M_{\text{ini}} & \text{in } \Omega_{ext}^\varepsilon, \end{cases}$$

where $\hat{\sigma}_\varepsilon = \hat{\sigma}(\frac{\mathbf{x}}{\varepsilon})$. Finally, we will assume that the time profile f belongs to $L^\infty(]0,T[)$ and that the initial data M_{ini} is defined on Ω independently of ε and it is constant in each compartment.

3. An asymptotic model. In this section, we derive the new asymptotic model.

3.1. Transformed Bloch–Torrey equation. As was already observed in [11], M_ε does not satisfy the Bloch–Torrey equation in all Ω_{ext}^ε, but only in Ω_e^ε and Ω_c^ε separately with jump conditions on the interfaces. We transform the Bloch–Torrey equation by defining a new unknown $\widetilde{M}_\varepsilon$ almost everywhere on $\mathbb{R}^d \times]0,T[$ by

$$\widetilde{M}_\varepsilon(\mathbf{x},t) = M_\varepsilon(\mathbf{x},t) e^{\iota q\, \mathbf{u_g}\cdot\mathbf{x}\, F(t)},$$

where

$$F(t) := \int_0^t f(s)ds.$$

Multiplying the equations of the system (2.6) by $e^{\iota q \mathbf{u_g}\cdot\mathbf{x}F(t)}$ and using the definition of $\widetilde{M}_\varepsilon$, we obtain the following transformed PDE:

(3.1)
$$\begin{cases} \dfrac{\partial}{\partial t}\widetilde{M}_\varepsilon(\mathbf{x},t) - \operatorname{div}\big(\hat{\sigma}_\varepsilon \nabla \widetilde{M}_\varepsilon(\mathbf{x},t) - \iota q \mathbf{u_g} F(t)\hat{\sigma}_\varepsilon \widetilde{M}_\varepsilon(\mathbf{x},t)\big) \\ \qquad + \ \iota q \mathbf{u_g} F(t)\hat{\sigma}_\varepsilon \nabla \widetilde{M}_\varepsilon(\mathbf{x},t) + q^2 F(t)^2 \hat{\sigma}_\varepsilon \widetilde{M}_\varepsilon(\mathbf{x},t) = 0 & \text{in } \Omega^\varepsilon_{ext}\times]0,T[\,, \\ \hat{\sigma}_\varepsilon \nabla \widetilde{M}_\varepsilon \cdot \nu - \iota q \mathbf{u_g} F(t)\hat{\sigma}_\varepsilon \widetilde{M}_\varepsilon \cdot \nu = \kappa^\varepsilon [\![\widetilde{M}_\varepsilon]\!]_{\Gamma^\varepsilon_m} & \text{on } \Gamma^\varepsilon_m\times]0,T[\,, \\ [\![\hat{\sigma}_\varepsilon \nabla \widetilde{M}_\varepsilon \cdot \nu - \iota q \mathbf{u_g} F(t)\hat{\sigma}_\varepsilon \widetilde{M}_\varepsilon \cdot \nu]\!]_{\Gamma^\varepsilon_m} = 0 & \text{on } \Gamma^\varepsilon_m\times]0,T[\,, \\ \widetilde{M}_\varepsilon(\cdot,0) = M_{\text{ini}} & \text{in } \Omega^\varepsilon_{ext}. \end{cases}$$

3.2. Choice of scaling. As explained previously, we have chosen the scaling of the periodicity length to be

$$L = \varepsilon L_0, \tag{3.2}$$

where L_0 has the unit of *length*. We note that ε is without dimension.

We keep the same scaling of the membrane permeability as was used in [11]:

$$\kappa = \varepsilon \kappa_0, \tag{3.3}$$

where κ_0 has the unit of *length/time*. Other scalings of permeability may be chosen (and lead to other asymptotic models), but because biological cell membranes impede the movement of water, the permeability should be "small." Certainly, a physically realistic choice should have the property that $\kappa^\varepsilon \to 0$ as $\varepsilon \to 0$.

Now we come to the choice of the scaling of b, which depends on both q and time (through the values of δ and Δ). We set the scaling of time to be

$$t = \varepsilon^\alpha \tau, \tag{3.4}$$

which implies

$$\delta = \varepsilon^\alpha \delta_0 \qquad \text{and} \qquad \Delta = \varepsilon^\alpha \Delta_0,$$

and F becomes

$$F_\varepsilon(t) = \varepsilon^\alpha F_0\left(\frac{t}{\varepsilon^\alpha}\right) = \varepsilon^\alpha F_0(\tau)\,.$$

We note that τ has the unit of *time*. We set the scaling of the gradient strength to be

$$q = \frac{q_0}{\varepsilon^\gamma}, \tag{3.5}$$

and q_0 has the unit of $\frac{1}{length\times time}$. In consequence, the scaling on b is

$$b = q^2 \int_0^{\Delta+\delta} F^2(t)dt = \frac{q_0^2}{\varepsilon^{2\gamma}}\varepsilon^{2\alpha}\delta_0^2\left(\varepsilon^\alpha\Delta_0 - \frac{\varepsilon^\alpha\delta_0}{3}\right) = \varepsilon^{3\alpha-2\gamma}b_0\,. \tag{3.6}$$

Before we choose the values of α and γ definitively, we use the periodic homogenization techniques [4] to develop $\widetilde{M}_\varepsilon$ using two-scale asymptotic expansions for Ω^ε_e

and Ω_c^ε, along with the new time scaling, for general α and γ. We write

$$\widetilde{M}_\varepsilon(\mathbf{x},t) = \begin{cases} \widetilde{M}_\varepsilon^e(\mathbf{x},t) = \displaystyle\sum_{i=0}^{\infty} \varepsilon^i \widetilde{M}_{ie}(\mathbf{x},\mathbf{y},\tau) & \text{in } Y_e, \\ \widetilde{M}_\varepsilon^c(\mathbf{x},t) = \displaystyle\sum_{i=0}^{\infty} \varepsilon^i \widetilde{M}_{ic}(\mathbf{x},\mathbf{y},\tau) & \text{in } Y_c, \end{cases} \tag{3.7}$$

where

$$\mathbf{y} = \frac{\mathbf{x}}{\varepsilon} \qquad \text{and} \qquad \tau = \frac{t}{\varepsilon^\alpha}$$

and the functions $\widetilde{M}_{ie}(\mathbf{x},\mathbf{y},\tau)$ and $\widetilde{M}_{ic}(\mathbf{x},\mathbf{y},\tau)$ are defined on $\Omega \times Y_e \times]0, T/\varepsilon^\alpha[$ and $\Omega \times Y_c \times]0, T/\varepsilon^\alpha[$, respectively, and the $\widetilde{M}_{ij}$ are assumed Y-periodic in $\mathbf{y}$. The aim of this ansatz is to obtain a new problem in which the different scales are linked.

To get the PDEs for each of the $\widetilde{M}_{ie}$ and the $\widetilde{M}_{ic}$, we start by noticing that for $j \in \{ c, e \}$,

$$\begin{aligned} \frac{\partial}{\partial t}\widetilde{M}_{ij}(\mathbf{x},\mathbf{y},\tau) &= \varepsilon^{-\alpha}\frac{\partial}{\partial \tau}\widetilde{M}_{ij}(\mathbf{x},\mathbf{y},\tau), \\ \nabla \widetilde{M}_{ij}(\mathbf{x},\mathbf{y},\tau) &= \nabla_{\mathbf{x}}\widetilde{M}_{ij}(\mathbf{x},\mathbf{y},\tau) + \varepsilon^{-1}\nabla_{\mathbf{y}}\widetilde{M}_{ij}(\mathbf{x},\mathbf{y},\tau), \end{aligned}$$

and therefore

$$\begin{aligned} &\operatorname{div}\big(\sigma_j(\mathbf{y})\nabla\widetilde{M}_{ij}(\mathbf{x},\mathbf{y},\tau) - \iota q \mathbf{u}_{\mathbf{g}} F(t)\sigma_j(\mathbf{y})\widetilde{M}_{ij}(\mathbf{x},\mathbf{y},\tau)\big) \\ &\qquad + \operatorname{div}_{\mathbf{x}}\big(\sigma_j(\mathbf{y})\nabla_{\mathbf{x}}\widetilde{M}_{ij}(\mathbf{x},\mathbf{y},\tau)\big) + \varepsilon^{-2}\operatorname{div}_{\mathbf{y}}\big(\sigma_j(\mathbf{y})\nabla_{\mathbf{y}}\widetilde{M}_{ij}(\mathbf{x},\mathbf{y},\tau)\big) \\ &\qquad + \varepsilon^{-1}\Big(\operatorname{div}_{\mathbf{y}}\big(\sigma_j(\mathbf{y})\nabla_{\mathbf{x}}\widetilde{M}_{ij}(\mathbf{x},\mathbf{y},\tau)\big) + \operatorname{div}_{\mathbf{x}}\big(\sigma_j(\mathbf{y})\nabla_{\mathbf{y}}\widetilde{M}_{ij}(\mathbf{x},\mathbf{y},\tau)\big)\Big) \\ &\qquad - \varepsilon^{\alpha-\gamma}\operatorname{div}_{\mathbf{x}}\big(\iota q_0 \mathbf{u}_{\mathbf{g}} F_0(\tau)\sigma_j(\mathbf{y})\widetilde{M}_{ij}(\mathbf{x},\mathbf{y},\tau)\big) \\ &\qquad - \varepsilon^{\alpha-\gamma-1}\operatorname{div}_{\mathbf{y}}\big(\iota q_0 \mathbf{u}_{\mathbf{g}} F_0(\tau)\sigma_j(\mathbf{y})\widetilde{M}_{ij}(\mathbf{x},\mathbf{y},\tau)\big). \end{aligned}$$

Substituting these relations into the transformed Bloch–Torrey PDE (3.1) and using the ansatz in (3.7), we obtain the following PDE for $j \in \{ c, e \}$:

$$\begin{aligned} &\sum_{i=0}^{\infty} \varepsilon^{i-\alpha}\frac{\partial}{\partial\tau}\widetilde{M}_{ij} + \varepsilon^{i+2\alpha-2\gamma} q_0^2 \mathbf{u}_{\mathbf{g}}\cdot\mathbf{u}_{\mathbf{g}} F_0(\tau)^2\sigma_j\widetilde{M}_{ij} \\ &\qquad + \varepsilon^{i+\alpha-\gamma}\iota q_0 \mathbf{u}_{\mathbf{g}} F_0(\tau)\sigma_j(\nabla_{\mathbf{x}}\widetilde{M}_{ij} + \varepsilon^{-1}\nabla_{\mathbf{y}}\widetilde{M}_{ij}) - \varepsilon^i\operatorname{div}_{\mathbf{x}}(\sigma_j\nabla_{\mathbf{x}}\widetilde{M}_{ij}) \\ &\qquad - \varepsilon^{i-1}\operatorname{div}_{\mathbf{x}}(\sigma_j\nabla_{\mathbf{y}}\widetilde{M}_{ij}) - \varepsilon^{i-1}\operatorname{div}_{\mathbf{y}}(\sigma_j\nabla_{\mathbf{x}}\widetilde{M}_{ij}) - \varepsilon^{i-2}\operatorname{div}_{\mathbf{y}}(\sigma_j\nabla_{\mathbf{y}}\widetilde{M}_{ij}) \\ &\qquad + \varepsilon^{i+\alpha-\gamma}\operatorname{div}_{\mathbf{x}}(\iota q_0 \mathbf{u}_{\mathbf{g}} F_0(\tau)\sigma_j\widetilde{M}_{ij}) + \varepsilon^{i+\alpha-\gamma-1}\operatorname{div}_{\mathbf{y}}(\iota q_0 \mathbf{u}_{\mathbf{g}} F_0(\tau)\sigma_j\widetilde{M}_{ij}) = 0. \end{aligned} \tag{3.8}$$

To obtain the analogous conditions for the traces, for $\mathbf{x} \in \Gamma_m^\varepsilon$, we write the ansatz for the jumps of $\widetilde{M}_\varepsilon$ and its fluxes,

$$[\![\widetilde{M}_\varepsilon(\mathbf{x},t)]\!]_{\Gamma_m^\varepsilon} = \sum_{i=0}^{\infty} \varepsilon^i\Big(\widetilde{M}_{ie}(\mathbf{x},\mathbf{y},\tau) - \widetilde{M}_{ic}(\mathbf{x},\mathbf{y},\tau)\Big) \tag{3.9}$$

and

$$
\begin{aligned}
(3.10)\quad &[\![\hat{\sigma}_\varepsilon \nabla \widetilde{M}_\varepsilon \cdot \nu - \iota q \mathbf{u_g} F \hat{\sigma}_\varepsilon \widetilde{M}_\varepsilon \cdot \nu]\!]_{\Gamma_m^\varepsilon} \\
&\quad = \sum_{i=0}^{\infty} \Big(\sigma_e \nabla \widetilde{M}_{ie}(\mathbf{x},\mathbf{y},\tau)\cdot\nu - \iota q_0 \mathbf{u_g} F_0(\tau)\sigma_e \widetilde{M}_{ie}(\mathbf{x},\mathbf{y},\tau)\cdot\nu \\
&\qquad\qquad - \sigma_c \nabla \widetilde{M}_{ic}(\mathbf{x},\mathbf{y},\tau)\cdot\nu - \iota q_0 \mathbf{u_g} F_0(\tau)\sigma_c \widetilde{M}_{ic}(\mathbf{x},\mathbf{y},\tau)\cdot\nu \Big).
\end{aligned}
$$

The conditions for the traces, $j \in \{e, c\}$, are then

$$
\begin{aligned}
\sum_{i=0}^{\infty} \varepsilon^{i+1} \kappa_0 \Big(\widetilde{M}_{ie} - \widetilde{M}_{ic} \Big) =& \varepsilon^{-1} \sigma_j \nabla_{\mathbf{y}} \widetilde{M}_{0j} \cdot \nu + \varepsilon^0 \Big(\sigma_j \nabla_{\mathbf{y}} \widetilde{M}_{1j} + \sigma_j \nabla_{\mathbf{x}} \widetilde{M}_{0j} - \iota q_0 \mathbf{u_g} F_0 \sigma_j \widetilde{M}_{0j} \Big) \cdot \nu \\
&+ \sum_{i=1}^{\infty} \varepsilon^i \Big(\sigma_j \nabla_{\mathbf{y}} \widetilde{M}_{i+1j} + \sigma_j \nabla_{\mathbf{x}} \widetilde{M}_{ij} - \iota q_0 \mathbf{u_g} F_0 \sigma_j \widetilde{M}_{ij} \Big) \cdot \nu \,. \qquad (3.11)
\end{aligned}
$$

The initial conditions, for $j \in \{e, c\}$, are

$$
\begin{aligned}
&\widetilde{M}_{0j}(\cdot,\cdot,0) = M_{\mathrm{ini}}, \\
&\widetilde{M}_{ij}(\cdot,\cdot,0) = 0 \qquad \forall i \geq 1.
\end{aligned}
$$

As our purpose was to find an accurate approximation of the (time-dependent) *ADC* for low b-values, whose scaling is

$$
b = \varepsilon^\theta b_0 \,, \qquad (3.12)
$$

where $\theta = 3\alpha - 2\gamma$, we require $\theta > 0$. We also need the time to be small since, if not, the effective diffusion would become Gaussian, and therefore the *ADC* would not be time-dependent. Hence we require that $\alpha > 0$.

Analyzing (3.8) we are led to choose α and γ so that the term $\varepsilon^{i+2\alpha-2\gamma} q_0^2 \mathbf{u_g} \cdot \mathbf{u_g} F_0^2 \sigma \widetilde{M}_{ij}$ appears in the early values of i since this is the term that contains quantities related to the b-value. The choice $\alpha = \gamma = 0$, which implies $b = O(1)$, was made in our previous work [11], which resulted in an *ADC* that is time-independent. We then tried $\alpha = \gamma = 1$, which implies $b = O(\varepsilon)$, but this choice also led to an *ADC* that is time-independent.

This means that the scaling in b is not sufficiently small. We thus proceeded to the scaling $b = O(\varepsilon^2)$, which resulted from the choice

$$
\alpha = \gamma = 2 \,. \qquad (3.13)
$$

For this choice, the interesting term appears in the PDE for $\widetilde{M}_{2j}$, $j \in \{e, c\}$. In what follows, we thus fix the choice of α and γ to be that in (3.13) and derive the corresponding asymptotic model.

3.3. Asymptotic model corresponding to $\alpha = \gamma = 2$. We recall that the functions $\widetilde{M}_{ie}(\mathbf{x},\mathbf{y},\tau)$ and $\widetilde{M}_{ic}(\mathbf{x},\mathbf{y},\tau)$ are defined on $\Omega \times Y_e \times]0, T/\varepsilon^\alpha[$ and $\Omega \times Y_c \times]0, T/\varepsilon^\alpha[$, respectively, and the $\widetilde{M}_{ij}$ are assumed Y-periodic in $\mathbf{y}$. To produce our new asymptotic model up to $O(\varepsilon^2)$, we substitute $\alpha = \gamma = 2$ and match the terms in front of the same power of ε of (3.8). We then get the following periodicity box problems for the first three orders: $i = 0, 1, 2$.

The problem for $\widetilde{M}_{0j}$ is then given by

$$\begin{cases} -\mathrm{div}_{\mathbf{y}}\big(\sigma_j \nabla_{\mathbf{y}} \widetilde{M}_{0j}\big) + \dfrac{\partial}{\partial \tau}\widetilde{M}_{0j} = 0 & \text{in } Y_j \times]0, T/\varepsilon^{\alpha}[\,, \\ \sigma_j \nabla_{\mathbf{y}} \widetilde{M}_{0j} \cdot \nu = 0 & \text{on } \Gamma_m, \\ \widetilde{M}_{0j}(\cdot, 0) = M_{\mathrm{ini}} & \text{in } Y_j, \\ \widetilde{M}_{0j} \text{ is } Y\text{-periodic.} \end{cases} \tag{3.14}$$

Since the initial conditions is constant, we deduce that

$$\widetilde{M}_{0j} \equiv M_{\mathrm{ini}}, \quad j \in \{\, e, c \,\}\,. \tag{3.15}$$

The periodic box problem for $\widetilde{M}_{1j}$ is

$$\begin{cases} -\mathrm{div}_{\mathbf{y}}\big(\sigma_j \nabla_{\mathbf{y}} \widetilde{M}_{1j} + \sigma_j \nabla_{\mathbf{x}} \widetilde{M}_{0j} - \iota q_0 \mathbf{u_g} F_0 \sigma_j \widetilde{M}_{0j}\big) = -\dfrac{\partial}{\partial \tau}\widetilde{M}_{1j} \\ \qquad\qquad - \iota q_0 \mathbf{u_g} F_0 \sigma_j \nabla_{\mathbf{y}} \widetilde{M}_{0j} + \mathrm{div}_{\mathbf{x}}\big(\sigma_j \nabla_{\mathbf{y}} \widetilde{M}_{0j}\big) & \text{in } Y_j \times]0, T/\varepsilon^{\alpha}[\,, \\ \sigma_j \nabla_{\mathbf{y}} \widetilde{M}_{1j} \cdot \nu + \sigma_j \nabla_{\mathbf{x}} \widetilde{M}_{0j} \cdot \nu - \iota q_0 \mathbf{u_g} F_0 \sigma_j \widetilde{M}_{0j} \cdot \nu = 0 & \text{on } \Gamma_m \times]0, T/\varepsilon^{\alpha}[\,, \\ \widetilde{M}_{1j}(\cdot, 0) = 0 & \text{in } Y_j, \\ \widetilde{M}_{1j} \text{ is } Y\text{-periodic,} \end{cases}$$

which, recalling that $\widetilde{M}_{0j}$ is a constant (3.15), simplifies to

$$\begin{cases} -\mathrm{div}_{\mathbf{y}}\big(\sigma_j \nabla_{\mathbf{y}} \widetilde{M}_{1j} - \iota q_0 \mathbf{u_g} F_0 \sigma_j M_{\mathrm{ini}}\big) = -\dfrac{\partial}{\partial \tau}\widetilde{M}_{1j} & \text{in } Y_j \times]0, T/\varepsilon^{\alpha}[\,, \\ \sigma_j \nabla_{\mathbf{y}} \widetilde{M}_{1j} \cdot \nu - \iota q_0 \mathbf{u_g} F_0 \sigma_j M_{\mathrm{ini}} \cdot \nu = 0 & \text{on } \Gamma_m \times]0, T/\varepsilon^{\alpha}[\,, \\ \widetilde{M}_{1j}(\cdot, 0) = 0 & \text{in } Y_j, \\ \widetilde{M}_{1j} \text{ is } Y\text{-periodic.} \end{cases} \tag{3.16}$$

It can be easily verified that $\widetilde{M}_{1j}$ is purely imaginary and that the imaginary part of $\widetilde{M}_{1j}$, for each $j \in \{c, e\}$, can be decomposed into the sum of d functions, ω_l^j, $l = 1, \ldots, d$, where d is the spatial dimension,

$$\Im\left(\widetilde{M}_{1j}(\mathbf{x}, \mathbf{y}, \tau)\right) = \sum_{l=1}^{d} (q_0 M_{\mathrm{ini}})\, \omega_l^j(\mathbf{y}, \tau)\, (\mathbf{u_g} \cdot \mathbf{e}_l) \qquad \text{in } Y_j\,, \tag{3.17}$$

where the ω_l^j's do not depend on the gradient direction $\mathbf{u_g}$ or q_0 and are solutions of

$$\begin{cases} -\mathrm{div}_{\mathbf{y}}\big(\sigma_j \nabla_{\mathbf{y}} \omega_l^j - F_0 \sigma_j \mathbf{e}_l\big) = -\dfrac{\partial}{\partial \tau}\omega_l^j & \text{in } Y_j \times]0, T/\varepsilon^{\alpha}[\,, \\ \sigma_j \nabla_{\mathbf{y}} \omega_l^j \cdot \nu - F_0 \sigma_j \mathbf{e}_l \cdot \nu = 0 & \text{on } \Gamma_m \times]0, T/\varepsilon^{\alpha}[\,, \\ \omega_l^j(\cdot, 0) = 0 & \text{in } Y_j, \\ \omega_l^j \text{ is } Y\text{-periodic.} \end{cases}$$

Now we consider the periodicity box problem satisfied by $\widetilde{M}_{2j}$:

(3.18)
$$\begin{cases} -\mathrm{div}_{\mathbf{y}}\big(\sigma_j\nabla_{\mathbf{y}}\widetilde{M}_{2j}+\sigma_j\nabla_{\mathbf{x}}\widetilde{M}_{1j}-\iota q_0\mathbf{u_g}F_0\sigma_j\widetilde{M}_{1j}\big)=-\dfrac{\partial}{\partial\tau}\widetilde{M}_{2j} & \text{in } Y_j\times]0,T/\varepsilon^\alpha[\\ \qquad -q_0^2F_0\sigma_j\widetilde{M}_{0j}-\iota q_0\mathbf{u_g}F_0\sigma_j\nabla_{\mathbf{y}}\widetilde{M}_{1j}\ -\iota q_0\mathbf{u_g}F_0\sigma_j\nabla_{\mathbf{x}}\widetilde{M}_{0j}\\ \qquad +\mathrm{div}_{\mathbf{x}}\big(\sigma_j\nabla_{\mathbf{y}}\widetilde{M}_{1j}+\sigma_j\nabla_{\mathbf{x}}\widetilde{M}_{0j}-\iota q_0\mathbf{u_g}F_0\sigma_j\widetilde{M}_{0j}\big),\\ \sigma_j\nabla_{\mathbf{y}}\widetilde{M}_{2j}\cdot\nu+\sigma_j\nabla_{\mathbf{x}}\widetilde{M}_{1j}\cdot\nu-\iota q_0\mathbf{u_g}F_0\sigma_j\widetilde{M}_{1j}\cdot\nu=\kappa_0\big(\widetilde{M}_{0e}-\widetilde{M}_{0c}\big) & \text{on } \Gamma_m\times]0,T/\varepsilon^\alpha[\,,\\ \widetilde{M}_{2j}(\cdot,0)=0 & \text{in } Y_j,\\ \widetilde{M}_{2j} \text{ is } Y\text{-periodic.} \end{cases}$$

Recalling again that $\widetilde{M}_{0j}\equiv M_{\mathrm{ini}}$ is constant in the whole domain, σ_j is piecewise constant, and $\widetilde{M}_{1j}$ is purely imaginary, we use the divergence theorem on the real part of (3.18) to obtain the compatibility condition for $\widetilde{M}_{2j}$ ($j\in\{e,c\}$):

$$-\int_{Y_j}\frac{\partial}{\partial\tau}\Re\left(\widetilde{M}_{2j}\right)-\int_{Y_j}q_0^2F_0^2\sigma_j\widetilde{M}_{0j}+\int_{Y_j}q_0\mathbf{u_g}F_0\sigma_j\nabla_{\mathbf{y}}\Im\left(\widetilde{M}_{1j}\right)=0\,.$$

Integrating in time, we obtain

(3.19)
$$\int_{Y_j}\Re\left(\widetilde{M}_{2j}\right)=-q_0^2\int_0^\tau F_0^2\int_{Y_j}\sigma_jM_{\mathrm{ini}}+q_0\mathbf{u_g}\sum_{l=1}^d\int_0^\tau F_0\int_{Y_j}\sigma_j\left(q_0M_{\mathrm{ini}}\right)\nabla_{\mathbf{y}}\omega_l^j\mathbf{u_g}\cdot\mathbf{e}_l\,.$$

We immediately remark that with the identical constant initial conditions for both compartments we lose the boundary term $\kappa_0(\widetilde{M}_{0e}-\widetilde{M}_{0c})$, which is the only information that we have on the membrane's permeability. This means that our model would not be applicable for situations where water exchange between the geometrical compartments is significant enough to affect the ADC, which is the first order moment with respect to q^2.

3.4. Asymptotic dMRI signal model and its *ADC*. In practice, the dMRI signal is measured at $t=T_E=\Delta+\delta$, so our reference signal is

$$S_{ref}(q,\mathbf{u_g})=\int M_\varepsilon(\mathbf{x},T_E)\,d\mathbf{x}\,,$$

where M_ε is the solution of the Bloch–Torrey PDE (2.6). The volume of integration above is assumed large enough to contain the support of the solution (again, we remind the reader that the voxel is large compared to diffusion displacement in dMRI). Then, remembering our ansatz (3.7) and the fact that we found the first three terms, the signal of our new asymptotic model is

$$\begin{aligned} S_{new}(q,\mathbf{u_g}) &:= \sum_{i=0}^2\varepsilon^i\bigg(\int_{Y_e}\widetilde{M}_{ie}(\cdot,T_E/\varepsilon^2)+\int_{Y_c}\widetilde{M}_{ic}(\cdot,T_E/\varepsilon^2)\bigg)\\ &= \int_{Y_e}\Big(M_{\mathrm{ini}}+\varepsilon^2\Re\widetilde{M}_{2e}(\cdot,T_E/\varepsilon^2)\Big)+\int_{Y_c}\Big(M_{\mathrm{ini}}+\varepsilon^2\Re\widetilde{M}_{2c}(\cdot,T_E/\varepsilon^2)\Big)\\ &= M_{\mathrm{ini}}\left(|Y_e|+|Y_e|\right)+\int_{Y_e}\varepsilon^2\Re\widetilde{M}_{2e}(\cdot,T_E/\varepsilon^2)+\int_{Y_c}\varepsilon^2\Re\widetilde{M}_{2c}(\cdot,T_E/\varepsilon^2). \end{aligned}$$

We recall that $\widetilde{M}_{0j}(\mathbf{x},\tau)=M_{\mathrm{ini}}$ in Y_j for all τ and the real part of $\widetilde{M}_{1j}$ is equal to zero, $j\in\{e,c\}$. Thus, our new model approximates the reference model up to fourth

order in ε (because the odd powers of ε are zero):

$$S_{ref}(q,\mathbf{u_g}) = S_{new}(q,\mathbf{u_g}) + O(\varepsilon^4).$$

Recalling (3.19), we define effective diffusion tensors in the geometrical compartments, $j \in \{c,e\}$, in the following way:

$$\left(\overline{D}_j^{eff}\right)_{il}(\tau) := \frac{1}{|Y_j|}\int_{Y_j}\sigma_j\left(\mathbf{e}_i\cdot\mathbf{e}_l - \frac{q_0^2\int_0^\tau F_0\frac{\partial}{\partial y_l}\omega_i^j}{b_0}\right), \quad i,l=1,\dots,d,$$

so that in more compact form,

$$\begin{aligned}\int_{Y_j}\Re\left(\widetilde{M}_{2j}\right) &= -q_0^2\int_0^\tau F_0^2\int_{Y_j}\sigma_j\ M_{\rm ini} + q_0\mathbf{u_g}\sum_{l=1}^d\int_0^\tau F_0\int_{Y_j}\sigma_j q_0 M_{\rm ini}\ \nabla_{\mathbf{y}}\omega_l^j\,(\mathbf{u_g}\cdot\mathbf{e}_l)\\ &= -M_{\rm ini}b_0\left(\int_{Y_j}\sigma_j - \mathbf{u_g}\sum_{l=1}^d\frac{q_0^2}{b_0}\int_0^\tau F_0\int_{Y_j}\sigma_j\nabla_{\mathbf{y}}\omega_l^j\,(\mathbf{u_g}\cdot\mathbf{e}_l)\right)\\ &= -M_{\rm ini}\,|Y_j|\,b_0\,\overline{D}_j^{eff}(\tau)\mathbf{u_g}\cdot\mathbf{u_g}\,.\end{aligned}$$

Now we simplify the signal after the normalization

$$M_{\rm ini} := \frac{1}{(|Y_c|+|Y_e|)},$$

$$S_{new}(q,\mathbf{u_g}) = 1 - \frac{\varepsilon^2 b_0\ \left(|Y_c|\,\overline{D}_c^{eff}(\Delta_0+\delta_0) + |Y_e|\,\overline{D}_e^{eff}(\Delta_0+\delta_0)\right)\mathbf{u_g}\cdot\mathbf{u_g}}{(|Y_c|+|Y_e|)},$$

and put back the original variables,

$$S_{new}(q,\mathbf{u_g}) = 1 - b\ \frac{\left(|Y_c|\,\overline{D}_c^{eff}(\Delta+\delta) + |Y_e|\,\overline{D}_e^{eff}(\Delta+\delta)\right)\mathbf{u_g}\cdot\mathbf{u_g}}{(|Y_c|+|Y_e|)}, \tag{3.20}$$

where the effective diffusion tensors in compartment $j\in\{c,e\}$ are

$$\left(\overline{D}_j^{eff}\right)_{il}(t) := \frac{1}{|Y_j|}\int_{Y_j}\sigma_j\ \mathbf{e}_i\cdot\mathbf{e}_l - \frac{1}{\int_0^{\Delta+\delta}F^2}\int_0^t\left(F\frac{1}{|Y_j|}\int_{Y_j}\sigma_j\frac{\partial}{\partial y_l}\omega_i^j\right),\ i,l=1,\dots,d, \tag{3.21}$$

and the periodicity box problems to be solved are

$$\begin{cases}\dfrac{\partial}{\partial t}\omega_l^j - \mathrm{div}_{\mathbf{y}}\left(\sigma_j\nabla_{\mathbf{y}}\omega_l^j - F\sigma_j\mathbf{e}_l\right) = 0 & \text{in } Y_j\times]0,T[\ ,\\ \sigma_j\nabla_{\mathbf{y}}\omega_l^j\cdot\nu - F\sigma_j\mathbf{e}_l\cdot\nu = 0 & \text{on } \Gamma_m\times]0,T[\ ,\\ \omega_l^j(\cdot,0) = 0 & \text{in } Y_j,\\ \omega_l^j \text{ is } Y\text{-periodic.}\end{cases} \tag{3.22}$$

From this simplified expression we can identify the ADC_{new} for this new model as

$$ADC_{new} := \theta_e\overline{D}_e^{eff}(\Delta+\delta)\mathbf{u_g}\cdot\mathbf{u_g} + \theta_c\overline{D}_c^{eff}(\Delta+\delta)\mathbf{u_g}\cdot\mathbf{u_g},\ \theta_c := \frac{|Y_c|}{|Y|}\,\theta_e := 1-\theta_c, \tag{3.23}$$

where θ_e and θ_c are the extracellular and intracellular volume fractions, respectively.

From (3.21) we immediately see that the definition of the effective diffusion tensor $\overline{D}_j^{eff}$, $j \in \{e, c\}$, is dependent on Δ and δ. In particular, $\overline{D}_j^{eff}$ is defined as the sum of two terms: the first is the intrinsic diffusion coefficient, and the second depends on the magnetic field gradient time profile $f(t)$ (in addition to depending on the geometry) and is bounded between 0 and σ_j.

Our new asymptotic model matched terms up to and including $O(\varepsilon^2)$, and since by the choice of the scaling our b-value is also $O(\varepsilon^2)$, this means that our model explains first order effects of the b-value; it does not account for higher order effects of b.

4. Numerical results. In this section, we first validate the fourth order convergence of our model (see (3.20), (3.21), (3.22)) in the signal and the second order convergence in the ADC (see (3.23)) to the reference Bloch–Torrey model of (2.6). Then we compare the ADC of our new model with the reference ADC as well as with two existing asymptotic models of the effective diffusion coefficient: the short time and long time models of (1.6) and (1.8).

In summary, the following quantities will be compared:

1. S_{ref} and ADC_{ref} from the reference Bloch–Torrey model.
2. S_{new} and ADC_{new} from our new asymptotic model.
3. D_{short}: the short time model of the effective diffusivity (see (1.6)).
4. $\overline{D}_{long}\mathbf{u_g} \cdot \mathbf{u_g}$: the long time model of the effective diffusivity (see (1.8)).

The reference signal is the integral of the solution of (2.6) in a periodic geometry, where the domain is made up of copies of the periodicity box $Y = [0, L]^2$. As was already observed in [29], equivalently, one can obtain the reference signal by solving (3.1) subject to periodic boundary conditions on ∂Y. This was also our approach here. The initial condition M_{ini} is set to $M_{\text{ini}} = 1/L^2$ to normalize the signal to $S = 1$ at $b = 0$. The ADC of the reference signal was then obtained using a polynomial fit of the logarithm of the simulated signal at several b-values according to (2.5).

To obtain the signal due to our new asymptotic model (see (3.20)), we solved the periodicity box problems (3.22) on Y. Then the ADC of our new model is computed according to (3.23).

To compute the long time model for the effective diffusivity according to (1.8), we solved the periodicity box problems (1.9).

The simulation of the reference model and the solution of the periodicity box problems were performed using FreeFem++ [34].

4.1. Convergence. We validate the convergence of the new model in a simple two-dimensional geometry. The periodicity box is $Y = [0, L]^2$, and we place in the center of Y a single disk of radius R (see Figure 1). We fix L_0, κ_0, Δ_0, δ_0, and b_0 and vary ε while respecting the scalings:

$$L = \varepsilon L_0, \quad \kappa = \varepsilon \kappa_0, \quad \Delta = \varepsilon^2 \Delta_0, \quad \delta = \varepsilon^2 \delta_0, \quad q = \varepsilon^{-2} q_0.$$

We recall that the above choice implies the scaling of $b = O(\varepsilon^2)$ and $\Delta = O(L^2)$. We have chosen the gradient direction to be $\mathbf{u_g} = \mathbf{e}_x$. Furthermore, our choices of L_0, κ_0, Δ_0, δ_0, and b_0 are made in order to obtain physically reasonable parameters L, κ, Δ, δ, and b at $\varepsilon = 0.25$.

We obtained S_{ref} and S_{new} using a very fine finite element mesh for two disk radii: $R = 0.49\,L$ and $R = 0.4\,L$. The values of the intrinsic diffusivities, $\sigma_e = 3 \times 10^{-3} mm^2/s$, $\sigma_c = 1.6 \times 10^{-3} mm^2/s$, were chosen close to the values often used

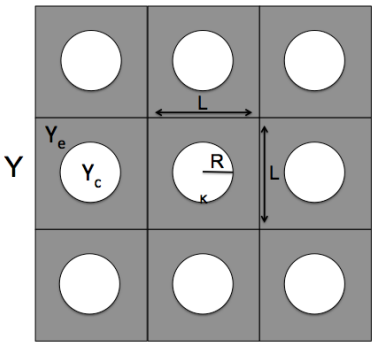

FIG. 1. *Illustration of a periodic domain where there is a disk of radius R in the center of each periodicity box Y.*

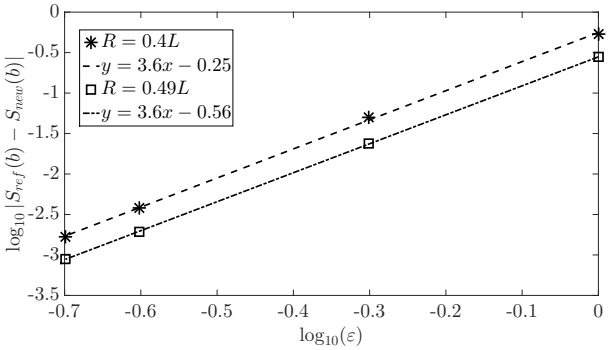

FIG. 2. *Signal convergence for a single disk in a periodicity box with $\sigma_e = 3 \times 10^{-3} mm^2/s$, $\sigma_c = 1.6 \times 10^{-3} mm^2/s$ for two disk radii: $R = 0.49\,L$ and $R = 0.4\,L$. $L_0 = 20\mu m$, $\delta_0 = 8ms$, $\Delta_0 = 8ms$, $b_0 = 800 s/mm^2$, and $\kappa_0 = 4 \times 10^{-5} m/s$.*

in the literature for dMRI numerical simulations [12, 45].

In Figure 2 we show the convergence of the signals $|S_{ref}(b) - S_{new}(b)|$ with the nondimensional parameter ε for two different choices of R. We see that the convergence rate is about 4 (fitted to 3.6).

In Figure 3 we show the convergence of the ADC with the nondimensional parameter ε, where to compute the reference ADC we use the linear fit:

$$ADC_{ref} \approx \frac{1 - S_{ref}(b)}{b}\,.$$

We see that the convergence rate is fitted to 1.6.

4.2. Time-dependent *ADC*. In this section we show some preliminary results on the ADC approximation of our new model (see (3.23)) and compare with some other existing models.

To compare the $ADCs$, we fixed $L = 5\mu m$, $\sigma_e = 3 \times 10^{-3} mm^2/s$, $\sigma_c = 1.6 \times 10^{-3} mm^2/s$, and $\kappa = 1 \times 10^{-5}$m/s, and we varied δ and Δ over a wide range. The simulated (δ, Δ), expressed in ms, are $(1e^{-3}, 5e^{-3})$, $(1e^{-3}, 10e^{-3})$, $(1e^{-3}, 15e^{-3})$, $(0.3, 0.3)$, $(0.5, 0.5)$, $(1.0, 1.0)$, $(1.5, 1.5)$, $(2.5, 2.5)$, $(2.5, 5.0)$, $(2.5, 7.5)$, $(2.5, 10.0)$, $(2.5, 15.0)$, $(2.5, 20.0)$, $(2.5, 40.0)$, and $(2.5, 80.0)$. The geometry is again a single

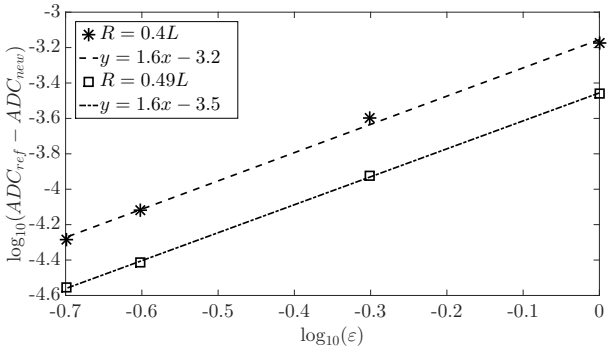

FIG. 3. *ADC convergence for a single disk in a periodicity box with* $\sigma_e = 3 \times 10^{-3} mm^2/s$, $\sigma_c = 1.6 \times 10^{-3} mm^2/s$ *for two disk radii:* $R = 0.49\,L$ *and* $R = 0.4\,L$. $L_0 = 20\mu m$, $\delta_0 = 8ms$, $\Delta_0 = 8ms$, $\kappa_0 = 4 \times 10^{-5} m/s$, *and fitted until* $b_0 = 800 s/mm^2$.

disk of different radii placed at the center of the periodicity box $Y = [0, L]^2$, and the gradient direction is $\mathbf{e}_x$. Two radii, $R = 0.49\,L$ and $R = 0.4\,L$, were simulated, in order to vary the volume fraction of the intracellular and extracellular compartments. The ADC_{ref} of the signal was obtained by a cubic fit using the logarithm of the signal at $b = 0, 10, 20, 40, 50 \text{s/mm}^2$.

Figure 4 displays a comparison of the $ADCs$ of the four different models as a function of the normalized diffusion displacement defined as

$$NDD := \frac{\sqrt{2(\Delta + \delta) ADC_{ref}}}{L/2}. \tag{4.1}$$

We immediately observe that the ADC_{new} of the new asymptotic model follows very well the reference model (2.6) in the whole range of NDD. On the other hand, as we expected, the long time model works well only when $NDD \gg 1$ and the short time model only when $NDD \ll 1$.

To validate our new asymptotic model in a more realistic geometry, we simulated a large periodic box, with $L = 50\mu m$, that contains many cells of different shapes and sizes. There are 32 spheres of various radii in the range of $[2.5, 5]\mu m$ and 5 cylinders of various radii in the range of $[0.7, 2]\mu m$ (Figure 5a). The resulting external volume fraction is then $\theta_e = 0.4$. We fixed $\sigma_e = 3 \times 10^{-3}\, mm^2/s$, $\sigma_c = 2 \times 10^{-3}\, mm^2/s$, and $\kappa = 1 \times 10^{-5}\,\text{m/s}$, and we varied δ and Δ over a wide range of times. The simulated (δ, Δ), expressed in ms, are $(0.1, 0.1)$, $(0.2, 0.2)$, $(0.3, 0.3)$, $(0.5, 0.5)$, $(1.0, 1.0)$, $(1.5, 1.5)$, $(2.5, 2.5)$, $(2.5, 5.0)$, $(2.5, 7.5)$, $(2.5, 10.0)$, $(2.5, 15.0)$, $(2.5, 20.0)$, $(2.5, 40.0)$, $(2.5, 80.0)$, $(2.5, 120.0)$, and $(2.5, 160.0)$. The gradient direction is $\mathbf{u_g} = [1/\sqrt{2}, 1/\sqrt{2}]$.

Figure 5b displays a comparison of the $ADCs$ of the four different models as a function of the diffusion displacement. In this example, we did not normalize the diffusion displacement by $L/2$ because the characteristic length of this domain is not obvious, given the presence of several cell shapes and sizes. The ADC_{ref} of the signal was obtained by a cubic fit using the logarithm of the signal at $b = 0, 20, 40, 60, 80, 100 \text{s/mm}^2$. We observe that the ADC_{new} of our new asymptotic model follows very well the reference model (2.6) in the whole range of diffusion displacement. On the contrary, as we expected, the short time model works well only for small

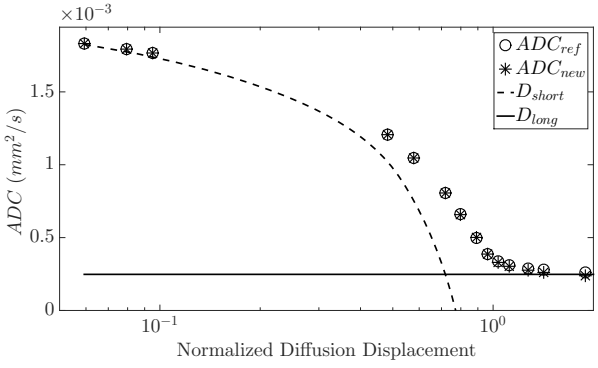

(a) $R = 0.49L$

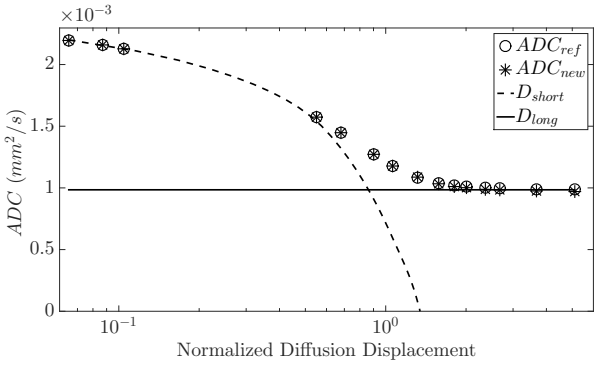

(b) $R = 0.4L$

FIG. 4. *ADC approximation for a single disk in a periodicity box with* $\kappa = 1 \times 10^{-5}\, m/s$, $\sigma_e = 3 \times 10^{-3} mm^2/s$, $\sigma_c = 1.6 \times 10^{-3} mm^2/s$, *for two disk radii:* $R = 0.49\, L$ *and* $R = 0.4\, L$.

diffusion displacement and the long time model only for large diffusion displacement. We see also that ADC_{ref} attains the long time limit at the diffusion displacement of around $10\mu m$, much smaller than $L/2$. This means the characteristic length of this medium is smaller than $L/2$, which is another reason we claim that the generality of our model is not limited by the original periodicity assumption on the domain when we performed the homogenization.

5. Conclusions. We have formulated a new asymptotic model of the dMRI signal from the Bloch–Torrey PDE using homogenization with a particular choice of scaling for the time, the biological cell membrane permeability, the diffusion-encoding magnetic field gradient strength, and a periodicity length of the cellular geometry. The apparent diffusion coefficient (ADC) of the resulting model is diffusion time–dependent, a property observed in in vivo imaging experiments of the brain. We numerically validated the new asymptotic model in two-dimensional geometrical configurations and showed that its ADC is close to the ADC of the reference Bloch–Torrey PDE model over a wide range of diffusion times. The derived model is valid for all dimensions. Numerical implementation in three dimensions, though most likely time-consuming, should be straightforward. Deeper analysis of this new model and adapting it to estimate model parameters from the dMRI signal data will be the subject of future work.

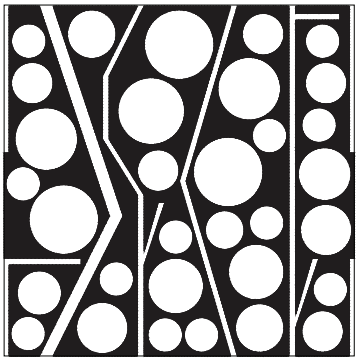

(a) Periodicity box $Y = [0, 50\mu m]^2$

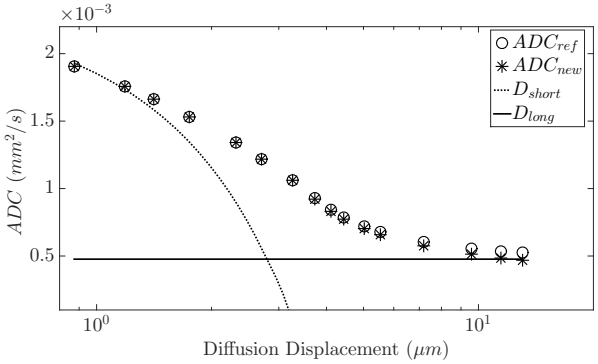

(b) Simulated ADC

FIG. 5. *ADC approximation for a periodic domain where the periodicity box* $Y = [0, 50\mu m]^2$ *is shown above. The extracellular volume fraction is* $\theta_e = 0.4$*, with the membrane permeability* $\kappa = 1 \times 10^{-5}\ m/s$*, and intrinsic diffusion coefficients:* $\sigma_e = 3 \times 10^{-3} mm^2/s$*, and* $\sigma_c = 2 \times 10^{-3} mm^2/s$.

REFERENCES

[1] T. ARBOGAST, *Gravitational forces in dual-porosity systems:* I. *Model derivation by homogenization*, Transp. Porous Media, 13 (1993), pp. 179–203, http://dx.doi.org/10.1007/BF00654409.

[2] T. ARBOGAST, *Gravitational forces in dual-porosity systems:* II. *Computational validation of the homogenized model*, Transp. Porous Media, 13 (1993), pp. 205–220, http://dx.doi.org/10.1007/BF00654410.

[3] Y. ASSAF, T. BLUMENFELD-KATZIR, Y. YOVEL, AND P. J. BASSER, *Axcaliber: A method for measuring axon diameter distribution from diffusion MRI*, Magn. Reson. Med., 59 (2008), pp. 1347–1354, http://dx.doi.org/10.1002/mrm.21577.

[4] A. BENSOUSSAN, J.-L. LIONS, AND G. PAPANICOLAOU, *Asymptotic Analysis for Periodic Structures*, Stud. Math. Appl. 5, North–Holland, Amsterdam, 1978.

[5] S. BHALEKAR, V. DAFTARDAR-GEJJI, D. BALEANU, AND R. MAGIN, *Generalized fractional order Bloch equation with extended delay*, Internat. J. Bifur. Chaos Appl. Sci. Engrg., 22 (2012), 1250071, http://dx.doi.org/10.1142/S021812741250071X.

[6] S. CHABERT, N. MOLKO, Y. COINTEPAS, P. LE ROUX, AND D. LE BIHAN, *Diffusion tensor imaging of the human optic nerve using a non-CPMG fast spin echo sequence*, J. Magn. Reson. Imaging, 22 (2005), pp. 307–310, http://dx.doi.org/10.1002/jmri.20383.

[7] J. CHEN, W. LIU, H. ZHANG, L. LACY, X. YANG, S.-K. SONG, S. A. WICKLINE, AND X. YU, *Regional ventricular wall thickening reflects changes in cardiac fiber and sheet structure during contraction: Quantification with diffusion tensor MRI*, Am. J. Physiol. Heart Circ. Physiol., 289 (2005), pp. H1898–H1907, http://dx.doi.org/10.1152/ajpheart.00041.2005.

[8] J. CHEN, S.-K. SONG, W. LIU, M. MCLEAN, J. S. ALLEN, J. TAN, S. A. WICKLINE, AND X. YU,

Remodeling of cardiac fiber structure after infarction in rats quantified with diffusion tensor MRI, Am. J. Physiol. Heart Circ. Physiol., 285 (2003), pp. H946–H954, http://dx.doi.org/10.1152/ajpheart.00889.2002.

[9] H. Cheng and S. Torquato, *Effective conductivity of periodic arrays of spheres with interfacial resistance*, Proc. Roy. Soc. London Ser. A, 453 (1997), pp. 145–161, http://dx.doi.org/10.1098/rspa.1997.0009.

[10] C. A. Clark and D. Le Bihan, *Water diffusion compartmentation and anisotropy at high b values in the human brain*, Magn. Reson. Med., 44 (2000), pp. 852–859, http://dx.doi.org/10.1002/1522-2594(200012)44:6%3C852::AID-MRM5%3E3.0.CO;2-A.

[11] J. Coatléven, H. Haddar, and J.-R. Li, *A macroscopic model including membrane exchange for diffusion MRI*, SIAM J. Appl. Math., 74 (2014), pp. 516–546, http://dx.doi.org/10.1137/130914255.

[12] K. D. Harkins, J.-P. Galons, T. W. Secomb, and T. P. Trouard, *Assessment of the effects of cellular tissue properties on ADC measurements by numerical simulation of water diffusion*, Magn. Reson. Med., 62 (2009), pp. 1414–1422, http://dx.doi.org/10.1002/mrm.22155.

[13] D. Hasselman and L. F. Johnson, *Effective thermal conductivity of composites with interfacial thermal barrier resistance*, J. Compos. Mater., 21 (1987), pp. 508–515.

[14] J. H. Jensen, J. A. Helpern, A. Ramani, H. Lu, and K. Kaczynski, *Diffusional kurtosis imaging: The quantification of non-Gaussian water diffusion by means of magnetic resonance imaging*, Magn. Reson. Med., 53 (2005), pp. 1432–1440, http://dx.doi.org/10.1002/mrm.20508.

[15] S. N. Jespersen, C. D. Kroenke, L. Astergaard, J. J. Ackerman, and D. A. Yablonskiy, *Modeling dendrite density from magnetic resonance diffusion measurements*, NeuroImage, 34 (2007), pp. 1473–1486, http://dx.doi.org/10.1016/j.neuroimage.2006.10.037.

[16] J. Karger, *NMR self-diffusion studies in heterogeneous systems*, Adv. Colloid Interface Sci., 23 (1985), pp. 129–148, http://dx.doi.org/10.1016/0001-8686(85)80018-X.

[17] L. L. Latour, K. Svoboda, P. P. Mitra, and C. H. Sotak, *Time-dependent diffusion of water in a biological model system*, Proc. Nat. Acad. Sci. U.S.A., 91 (1994), pp. 1229–1233, http://dx.doi.org/10.1073/pnas.91.4.1229.

[18] M. Lazar, *Mapping brain anatomical connectivity using white matter tractography*, NMR Biomed., 23 (2010), pp. 821–835, http://dx.doi.org/10.1002/nbm.1579.

[19] D. Le Bihan, E. Breton, D. Lallemand, P. Grenier, E. Cabanis, and M. Laval-Jeantet, *MR imaging of intravoxel incoherent motions: Application to diffusion and perfusion in neurologic disorders*, Radiology, 161 (1986), pp. 401–407, http://dx.doi.org/10.1148/radiology.161.2.3763909.

[20] D. Le Bihan and H. Johansen-Berg, *Diffusion MRI at* 25: *Exploring brain tissue structure and function*, NeuroImage, 61 (2012), pp. 324–341, http://dx.doi.org/10.1016/j.neuroimage.2011.11.006.

[21] D. LeBihan, S.-i. Urayama, T. Aso, T. Hanakawa, and H. Fukuyama, *Direct and fast detection of neuronal activation in the human brain with diffusion MRI*, Proc. Natl. Acad. Sci. USA, 103 (2006), pp. 8263–8268, http://dx.doi.org/10.1073/pnas.0600644103.

[22] R. Magin, X. Feng, and D. Baleanu, *Solving the fractional order Bloch equation*, Concept. Magn. Reson. A, 34A (2009), pp. 16–23, http://dx.doi.org/10.1002/cmr.a.20129.

[23] R. L. Magin, O. Abdullah, D. Baleanu, and X. J. Zhou, *Anomalous diffusion expressed through fractional order differential operators in the Bloch-Torrey equation*, J. Magn. Reson., 190 (2008), pp. 255–270, http://dx.doi.org/10.1016/j.jmr.2007.11.007.

[24] S. E. Maier, P. Bogner, G. Bajzik, H. Mamata, Y. Mamata, I. Repa, F. A. Jolesz, and R. V. Mulkern, *Normal brain and brain tumor: Multicomponent apparent diffusion coefficient line scan imaging*, Radiology, 219 (2001), pp. 842–849, http://dx.doi.org/10.1148/radiology.219.3.r01jn02842.

[25] S. E. Maier, Y. Sun, and R. V. Mulkern, *Diffusion imaging of brain tumors*, NMR Biomed., 23 (2010), pp. 849–864, http://dx.doi.org/10.1002/nbm.1544.

[26] P. P. Mitra, P. N. Sen, L. M. Schwartz, and P. Le Doussal, *Diffusion propagator as a probe of the structure of porous media*, Phys. Rev. Lett., 68 (1992), pp. 3555–3558.

[27] M. Moseley, J. Kucharczyk, J. Mintorovitch, Y. Cohen, J. Kurhanewicz, N. Derugin, H. Asgari, and D. Norman, *Diffusion-weighted MR imaging of acute stroke: Correlation with T2-weighted and magnetic susceptibility-enhanced MR imaging in cats*, AJNR Am. J. Neuroradiol., 11 (1990), pp. 423–429, http://www.ajnr.org/cgi/content/abstract/11/3/423.

[28] R. V. Mulkern, H. Gudbjartsson, C.-F. Westin, H. P. Zengingonul, W. Gartner, C. R. G. Guttmann, R. L. Robertson, W. Kyriakos, R. Schwartz, D. Holtz-

man, F. A. Jolesz, and S. E. Maier, *Multi-component apparent diffusion coefficients in human brain*, NMR Biomed., 12 (1999), pp. 51–62, http://dx.doi.org/10.1002/(SICI)1099-1492(199902)12:1%3C51::AID-NBM546%3E3.0.CO;2-E.

[29] D. V. Nguyen, J.-R. Li, D. Grebenkov, and D. Le Bihan, *A finite elements method to solve the Bloch-Torrey equation applied to diffusion magnetic resonance imaging*, J. Comput. Phys., 263 (2014), pp. 283–302, http://dx.doi.org/10.1016/j.jcp.2014.01.009.

[30] T. Niendorf, R. M. Dijkhuizen, D. G. Norris, M. van Lookeren Campagne, and K. Nicolay, *Biexponential diffusion attenuation in various states of brain tissue: Implications for diffusion-weighted imaging*, Magn. Reson. Med., 36 (1996), pp. 847–857, http://dx.doi.org/10.1002/mrm.1910360607.

[31] D. S. Novikov, E. Fieremans, J. H. Jensen, and J. A. Helpern, *Random walks with barriers*, Nat. Phys., 7 (2011), pp. 508–514, http://dx.doi.org/10.1038/nphys1936.

[32] D. S. Novikov, J. H. Jensen, J. A. Helpern, and E. Fieremans, *Revealing mesoscopic structural universality with diffusion*, Proc. Natl. Acad. Sci. USA, 111 (2014), pp. 5088–5093, http://dx.doi.org/10.1073/pnas.1316944111.

[33] D. S. Novikov and V. G. Kiselev, *Effective medium theory of a diffusion-weighted signal*, NMR Biomed., 23 (2010), pp. 682–697, http://dx.doi.org/10.1002/nbm.1584.

[34] O. Pironneau, F. Hecht, and J. Morice, *freefem++*, www.freefem.org/.

[35] N. Pyatigorskaya, D. Le Bihan, O. Reynaud, and L. Ciobanu, *Relationship between the diffusion time and the diffusion MRI signal observed at* 17.2 *tesla in the healthy rat brain cortex*, Magn. Reson. Med., 72 (2014), pp. 492–500, http://dx.doi.org/10.1002/mrm.24921.

[36] D. Rohmer, A. Sitek, and G. T. Gullberg, *Reconstruction and visualization of fiber and laminar structure in the normal human heart from ex vivo diffusion tensor magnetic resonance imaging (DTMRI) data*, Invest. Radiol., 42 (2007), pp. 777–789, PubMed:18030201.

[37] P. N. Sen and P. J. Basser, *A model for diffusion in white matter in the brain*, Biophys. J., 89 (2005), pp. 2927–2938, http://dx.doi.org/10.1529/biophysj.105.063016.

[38] E. O. Stejskal and J. E. Tanner, *Spin diffusion measurements: Spin echoes in the presence of a time-dependent field gradient*, J. Chem. Phys., 42 (1965), pp. 288–292, http://dx.doi.org/10.1063/1.1695690.

[39] T. Sugahara, Y. Korogi, M. Kochi, I. Ikushima, Y. Shigematu, T. Hirai, T. Okuda, L. Liang, Y. Ge, Y. Komohara, Y. Ushio, and M. Takahashi, *Usefulness of diffusion-weighted MRI with echo-planar technique in the evaluation of cellularity in gliomas*, J. Magn. Reson. Imaging, 9 (1999), pp. 53–60, http://dx.doi.org/10.1002/(SICI)1522-2586(199901)9:1%3C53::AID-JMRI7%3E3.0.CO;2-2.

[40] A. Szafer, J. Zhong, and J. C. Gore, *Theoretical model for water diffusion in tissues*, Magn. Reson. Med., 33 (1995), pp. 697–712, http://dx.doi.org/10.1002/mrm.1910330516.

[41] S. Torquato and M. D. Rintoul, *Effect of the interface on the properties of composite media*, Phys. Rev. Lett., 75 (1995), pp. 4067–4070, http://dx.doi.org/10.1103/PhysRevLett.76.3241.

[42] H. Torrey, *Bloch equations with diffusion terms*, Physical Review Online Archive (Prola), 104 (1956), pp. 563–565, http://dx.doi.org/10.1103/PhysRev.104.563.

[43] Y. Tsushima, A. Takahashi-Taketomi, and K. Endo, *Magnetic resonance (MR) differential diagnosis of breast tumors using apparent diffusion coefficient (ADC) on* 1.5-*t*, J. Magn. Reson. Imaging, 30 (2009), pp. 249–255, http://dx.doi.org/10.1002/jmri.21854.

[44] S. Warach, D. Chien, W. Li, M. Ronthal, and R. R. Edelman, *Fast magnetic resonance diffusion-weighted imaging of acute human stroke*, Neurology, 42 (1992), pp. 1717–1723, http://dx.doi.org/10.1212/WNL.42.9.1717.

[45] J. Xu, M. Does, and J. Gore, *Numerical study of water diffusion in biological tissues using an improved finite difference method*, Phys. Med. Biol., 52 (2007), pp. N111–N126, PubMed:17374905.

[46] D. Yablonskiy, L. Bretthorst, and J. Ackerman, *Statistical model for diffusion attenuated MR signal*, Magn. Reson. Med., 50 (2003), pp. 664–669, http://dx.doi.org/10.1002/mrm.10578.